Digital Holography and Applications in Microscopic Interferometry

Cody Jenkins
Dept. of Physics, California Polytechnic State University, San Luis Obispo
E-mail: cbjenkin@calpoly.edu

Abstract
In this project I demonstrate recording holograms using an electronic camera as the photosensitive element and subsequent numerical reconstruction in a digital computer. The technique is employed to show extended depth of field imaging as well as phase contrast imaging via microscopic interferometry.

1. Theory

1.1. Traditional Transmission Holography

In a traditional hologram setup, a beam of coherent, monochromatic light (from a HeNe laser source, for example) is passed into an optical system and split into two beams: an object beam and a reference beam. These beams are expanded and then re-collimated. The reference beam travels through the optical system unobstructed, while the object beam passes through one or more opaque and semitransparent objects in the path of the beam. The two beams are then mixed together on a photographic film. (see figure 1.1.1)

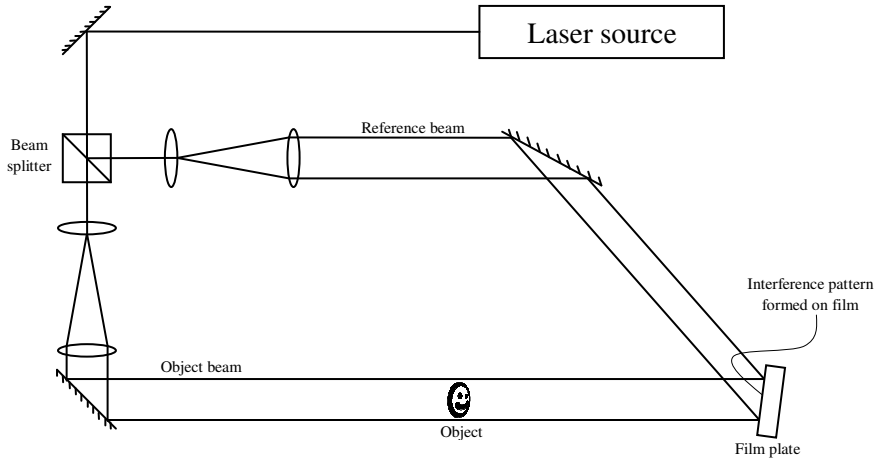

Figure 1.1.1 *Schematic design of a typical transmission holography setup*

When the beams are recombined, an interference pattern results and is recorded onto the film. After the film is developed, the points on the emulsion where constructive interference occurred are darkened and the points where destructive interference occurred are transparent. This interference pattern is an exact compliment to the interference pattern produced by the recombined beams, and the features are small enough to cause diffraction of coherent, monochromatic light. The pattern on the film is a hologram. When coherent light of the same wavelength is passed through the hologram on the film, the beam is diffracted in such a way as to approximately reconstruct the object beam as it would have been as it passed the film plane in the absence of the reference beam. (see figure 1.1.2)

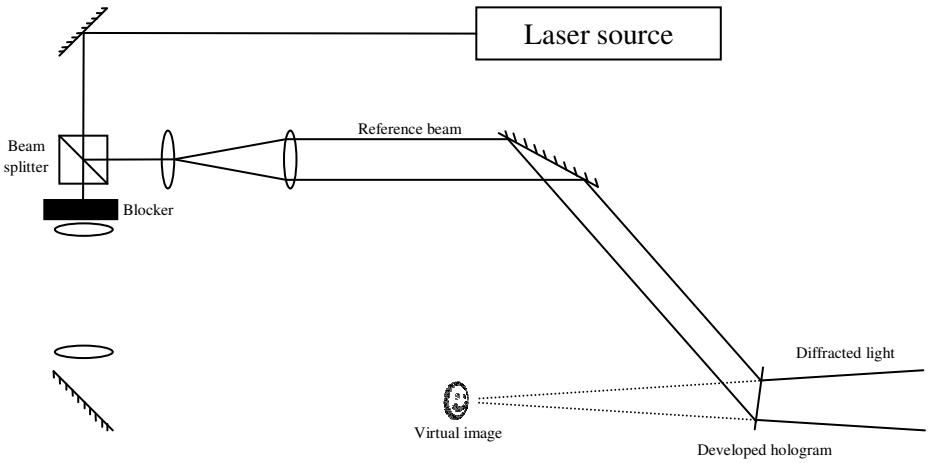

Figure 1.1.2 *"Replaying" of a transmission hologram; note the virtual image that is present where the object was relative to the film during the construction of the hologram*

Advances in modern electronics opened up the possibility of replacing photographic emulsion films with charge-coupled devices (CCDs) in holography setups. With a CCD, a holographer could create a hologram setup as described above, but instead record the hologram pattern in digital form to a computer for later analysis. As the processing power of computers increased, it also became feasible to reconstruct the object beam using numerical methods rather than by using physical diffraction.

1.2. The Fresnel-Kirchhoff Integral and Digital Holography

One such method of reconstructing the object beam's light field makes of the Fresnel-Kirchhoff integral shown below in equation 1.1

$$\Gamma(\xi,\eta) = \frac{\mathrm{i}}{\lambda}\int_{-\infty}^{\infty}\int_{-\infty}^{\infty} h(x,y)R(x,y)\frac{\exp\left(-i\frac{2\pi}{\lambda}\rho\right)}{\rho}\times\left(\frac{1}{2}+\frac{1}{2}\cos\theta\right)\mathrm{d}x\ \mathrm{d}y \tag{1.1}$$

where

$$\rho = \sqrt{(x-\xi)^2+(y-\eta)^2+d^2} \tag{1.2}$$

There are a lot of pieces, so we will go through each:

ξ,η	Coordinate system in the reconstruction plane
x,y	Coordinate system in the hologram plane
$\Gamma(\xi,\eta)$	The field distribution of the reconstruction; this is what we calculate to reconstruct an image from a hologram
$h(x,y)$	The amplitude transmittance of the hologram
$R(x,y)$	The field distribution of the reference wave. For our setup, we will simply use unity

ρ	The distance between a point in the hologram plane and a point in the reconstruction plane
θ	The angle between the optical axis and the line segment drawn from (x, y) in the hologram plane to (ξ, η) in the reconstruction plane
λ	The wavelength of the laser source; this is 633nm in our setup
d	The distance from the hologram to the reconstruction plane

The Fresnel-Kirchhoff integral may be adapted to be used in a computational setting by making some simplifications and other substitutions that are detailed in the referenced review article by Schnars and Jüptner [1]. For the sake of brevity, we will skip to the final equation used to compute an image from a digital hologram:

$$\Gamma(m,n) = \frac{\mathrm{i}}{\lambda d}\exp\left[-i\pi\,\lambda d\left(\frac{m^2}{M^2\Delta x^2}+\frac{n^2}{N^2\Delta y^2}\right)\right] \times \sum_{k=0}^{M-1}\sum_{l=0}^{N-1} R(k,l)\,h(k,l)\exp\left[-i\frac{\pi}{\lambda d}(k^2\Delta x^2 + l^2\Delta y^2)\right] \times \exp\left[\mathrm{i}2\pi\left(\frac{km}{M}+\frac{ln}{N}\right)\right] \tag{1.3}$$

One additional element that Schnars and Jüptner include in their equation is a "numerical" imaging lens to bring the light diffracted from the hologram to a focus forming a real image in the *m, n* plane. The arguments m and n in the function $\Gamma(m,n)$ are integer pixel coordinates of a point in a digital representation of that image. M and N are the width and height respectively of the digital hologram image in pixels. Δx and Δy are the horizontal and vertical widths respectively of the CCD pixels. λ is the wavelength of the laser used to expose the CCD. d is a parameter that we will vary depending on the distance between the image focal plane we wish to resolve and the CCD. We created a MATLAB algorithm to compute this numerical integral given an input hologram. It is attached in appendix A.

1.3. Microscopic Interferometry

The interference pattern caused by the intersection of the object and reference beams may also be used to measure the depth profile or optical thickness of a transparent object. This measurement technique is known as microscopic interferometry. Again, a beam of coherent, monochromatic light is split into an object beam and a reference beam. The reference beam travels through the optical system unobstructed, while the object beam passes through a transparent object in its path. The two beams are then recombined and directed towards a recording medium. However, in this setup, the light passing through the sample must come to a focus on the CCD.

In the image of the transparent sample, the interference pattern shifts depending on the optical thickness. It is possible to determine the phase shift introduced by a path through the transparent object directly by comparing the positions of the shifted fringes with the positions original fringes. We may infer the optical thickness of the object at a point in the interference pattern using equation 1.4.

$$d = \frac{m\lambda}{n_2 - n_1} \tag{1.4}$$

Here, *m* is the number of cycles the phase was retarded by, λ is the wavelength of the light, n_2 is the refractive index of the sample material, and n_1 is the refractive index of the surroundings of the material.

If the object beam is unobstructed, the intersecting object and reference beams produce an interference pattern like the one in figure 1.3.1.

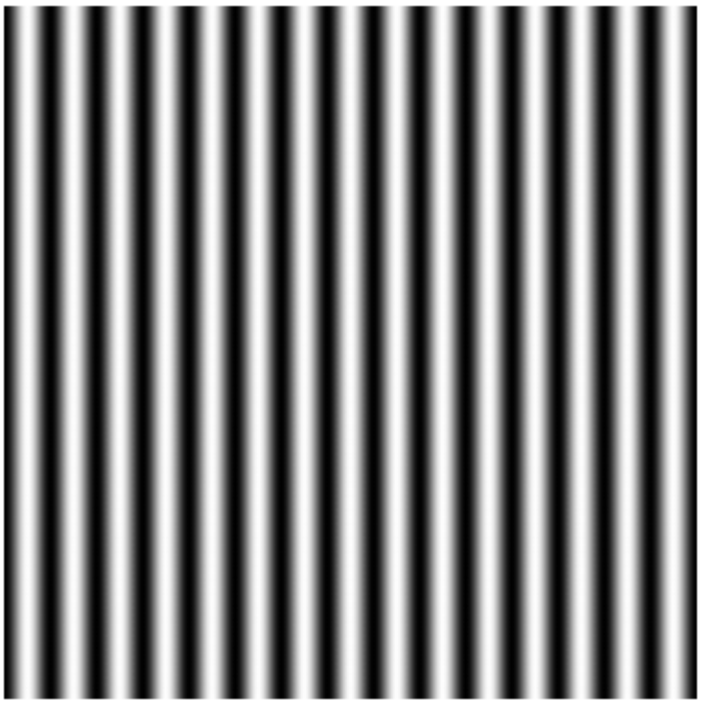

Figure 1.3.1 *Simulated interference pattern of intersecting reference beam and unobstructed object beam (simulation code in Appendix B)*

However, introducing a transparent sample into the path of the object beam causes the phase of the light from the object beam to shift slightly depending on the thickness of the object and its average refractive index. As stated before, this phase shift in the object beam causes the interference pattern to shift slightly. The shift in phase at a point on the recording medium is directly proportional to the optical thickness of the object at that point. For example, a transparent sphere sample optically thick at its center and optically thin at its edges. The shift in the interference pattern may look something like that in figure 1.3.2

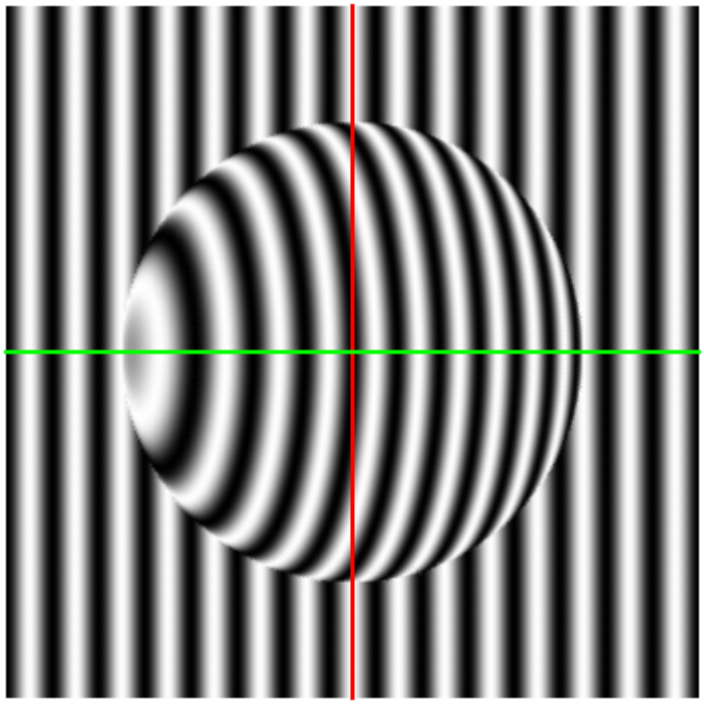

Figure 1.3.2 *Simulated interference pattern with a transparent, spherical obstruction in the object beam. The red line denotes the vertical center and the green line denotes the horizontal center (simulation code in Appendix C)*

The red line in figure 1.3.3 initially runs through a bright fringe at the top of the image. This bright fringe "bends" away from the red line reaching a maximum displacement at the horizontal center of the image along the green line. Moving back from this point towards the red line in the horizontal direction, we count a dark fringe, a bright fringe, and a final dark fringe. The light passing through the center of the sphere, then, must have had its phase retarded by 1.5 cycles.

2. Experiment

2.1. Recording and Reconstructing a transmission Hologram

We prepared our optical system as shown below in figure 2.1.1. In this setup, the vertically polarized HeNe beam is split into the usual reference and object beams. The reference beam is expanded and collimated before being recombined with the object beam at the second beam splitter. The object beam is expanded and collimated before passing through the sample and finally through the second beam splitter. Information about the CCD used, the capture software, and capture machine may be found in Appendix D.

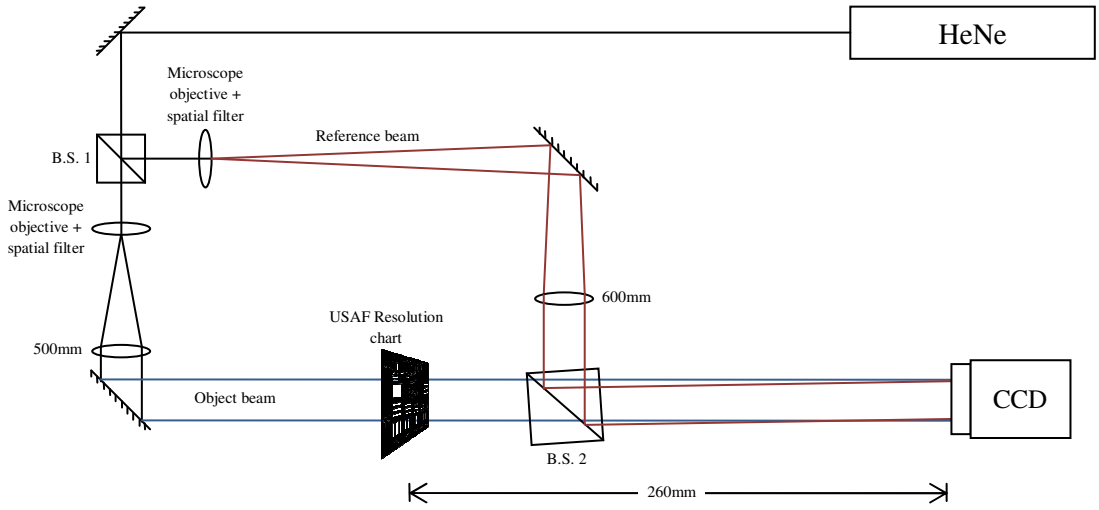

Figure 2.1.1 *Our slightly off-axis transmission holography optical setup. Drawing not to scale.*

The object beam is oriented such that the path of the object beam is at a slight angle to the reference beam. To make the calculation of the image simpler, it is assumed that this angle is small enough that the $\cos\theta$ term from equation 1.1 is approximately 1. The interference of an unobstructed object beam and the reference beam produces the interference pattern shown previously in figure 1.3.2.

We placed a USAF resolution chart in the path of the object beam and recorded the hologram shown in figure 2.1.3

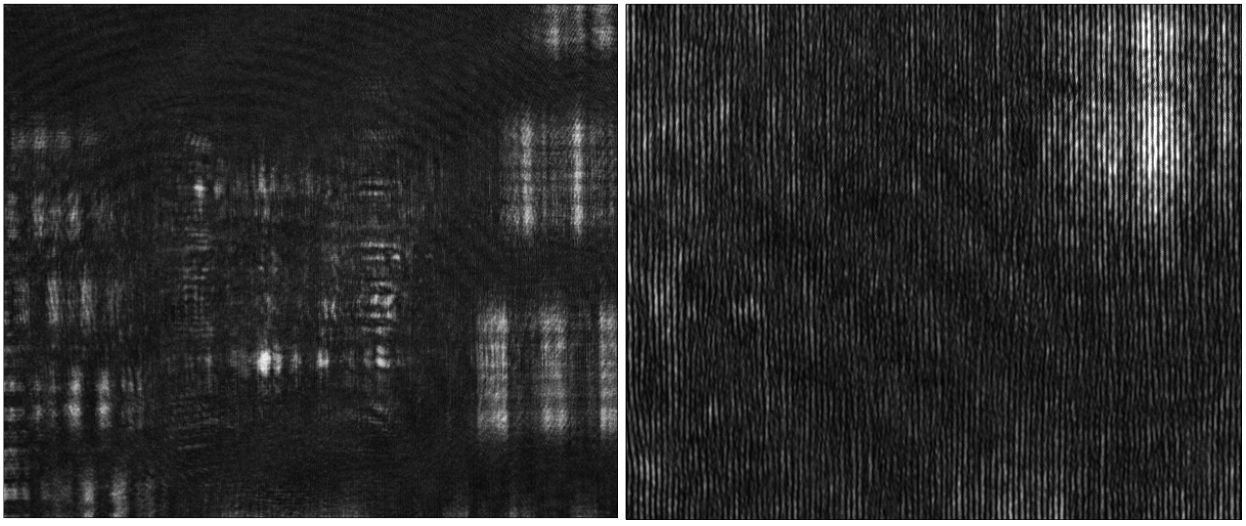

Figure 2.1.3 *Hologram of the USAF resolution chart as recoreded by the CCD. On the left is the full hologram. On the right is a small section of the hologram from the left showing the interference pattern detail.*

We then used the MATLAB program in Appendix A to compute the intensity of the light field on various focal planes near and parallel to the resolution chart. By varying the parameter *d* (the distance from the focal plane to the hologram plane) we could specify the focal plane we wished to observe. Figure 2.1.4 shows several images that we computed using different values of the parameter *d*. Notice the chart coming into and then going out of focus.

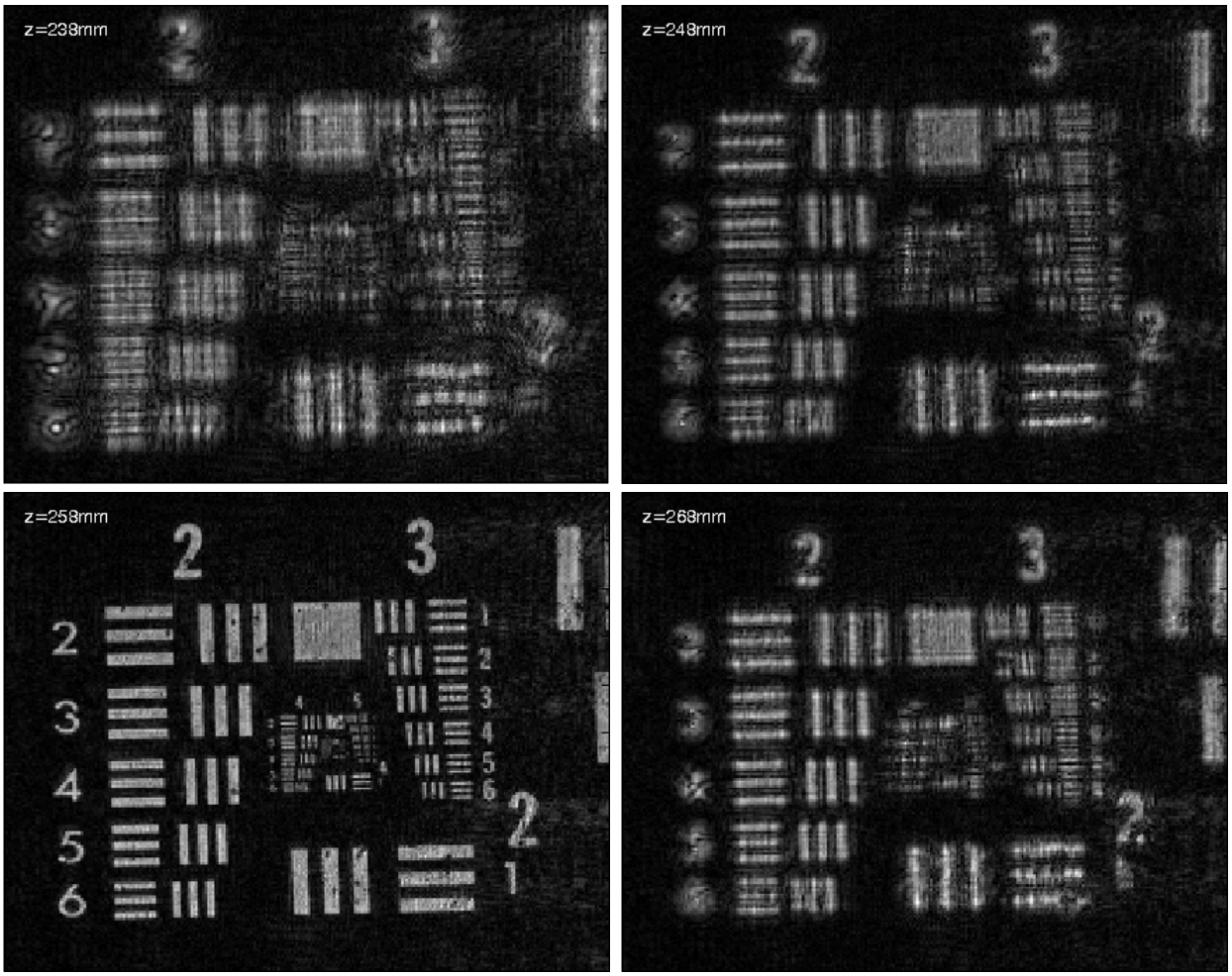

Figure 2.1.4 *Images computed by the MATLAB program using the Fresnel-Kirchhoff integral method. The image of the resolution chart comes into focus at 258mm and goes back out of focus past that point. In these images,* z *corresponds to the hologram-focal plane distance parameter* d*. At 258mm we see Groups 2, 3, and 4 clearly. The finest element that we were able to resolve from this hologram was Group 4 Element 3 which has a resolution of 20.16 line pairs per millimeter. That translates to a separation between bars of less than 25μm.*

The ability to select the focal plane allows us to resolve different parts of a 3-D sample using a single hologram. To demonstrate this principle, we prepared a set of four small semitransparent “flags” arrange one behind the other as shown in figure 2.1.5.

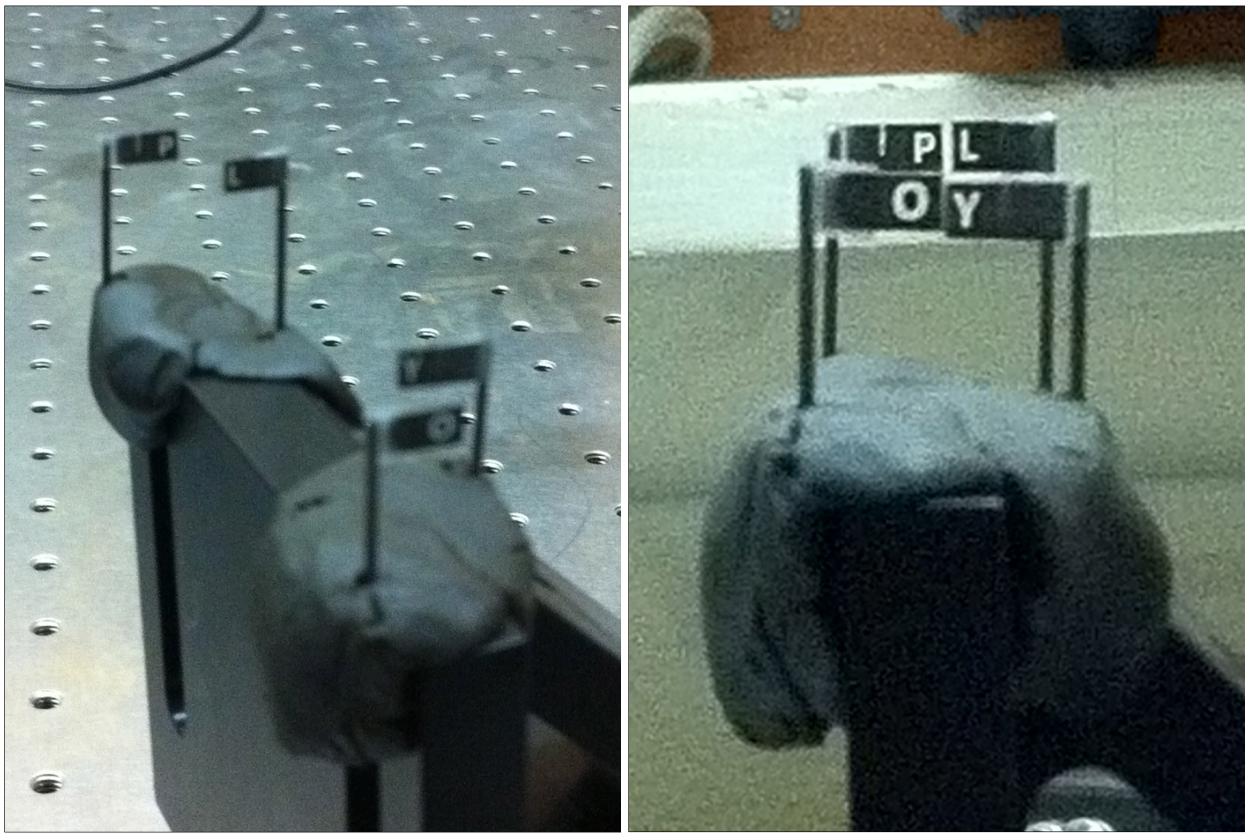

Figure 2.1.5 *Four small “flags” with transparent letters and opaque surroundings arranged at various position. The letters spell out “POLY”. From farthest to nearest, the letters are P, L, Y, O.*

We introduced this set of flags into the object beam as we did with the USAF resolution chart and captured the hologram shown in figure 2.1.6.

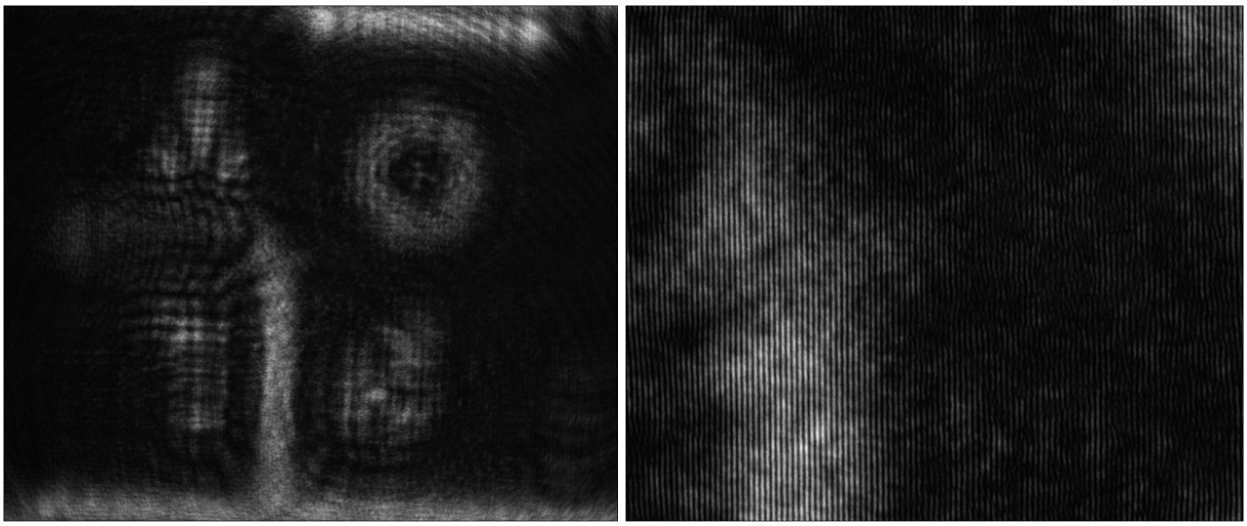

Figure 2.1.6 *Hologram produced with POLY flags. On the left is the full POLY hologram. On the right is a small section of the hologram from the left showing the interference pattern detail.*

We ran this hologram through the same MATLAB program and varied *d* to focus on each flag. Figure 2.1.7 shows the computed images with each of the letters of "POLY" in focus.

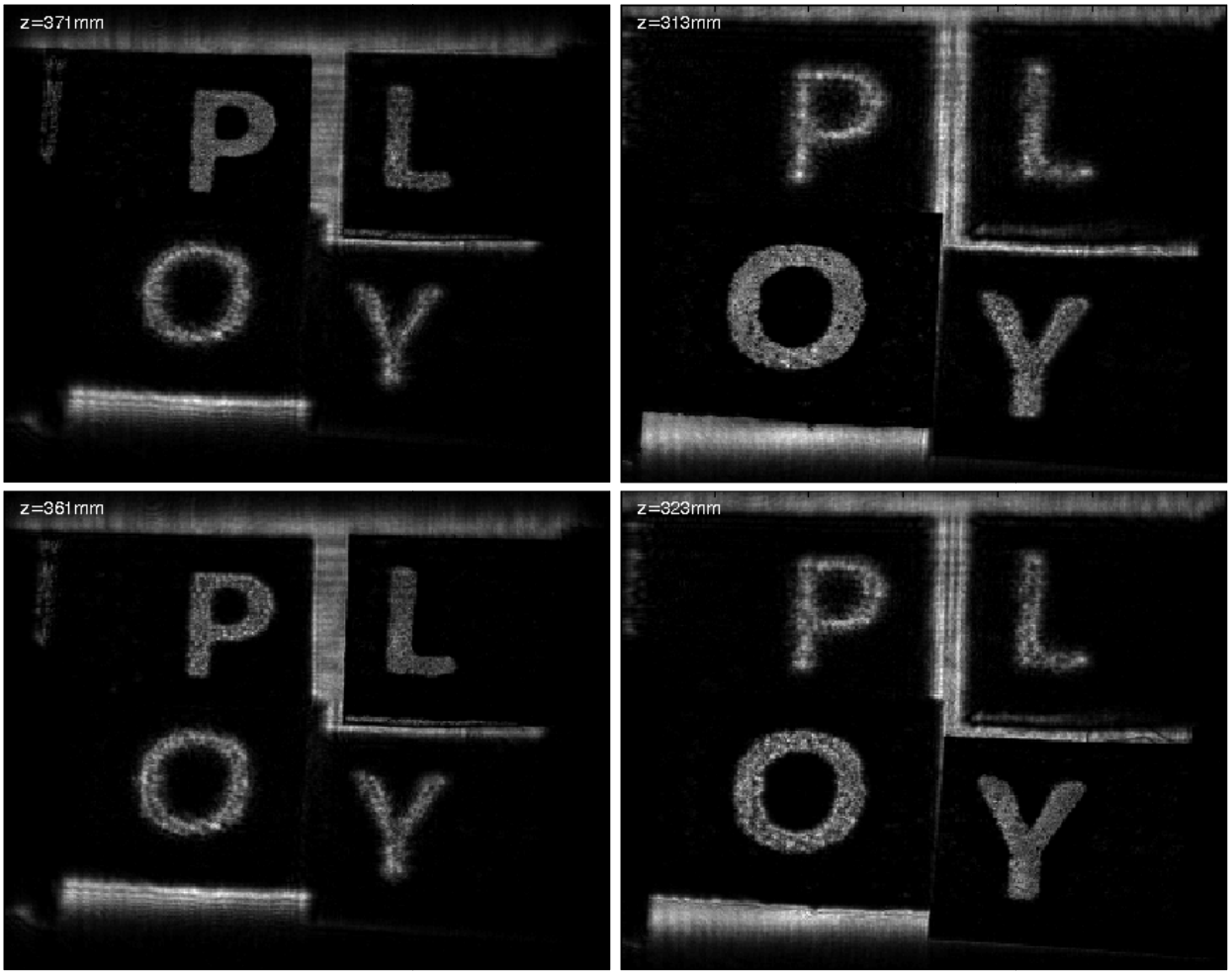

Figure 2.1.7 *Each of the four letters in focus as computed by the MATLAB program. In these images,* z *corresponds to the hologram-focal plane distance parameter* d.

It should be noted that these four images were generated from the same hologram. This emphasizes the idea that a hologram contains information about the whole light field around the sample and not just a single focal plane.

2.2. Microscopic Interferometry

The setup for microscopic interferometry is slightly different than for transmission holography, but many components are the same. Figure 2.2.1 shows our setup. The main difference is the introduction of the "Imaging lens" (as shown in the figure just after B.S. 2) in front of the CCD to image the sample onto the CCD. The reference beam must be refocused after its expansion, then, so that the CCD lens collimates the light from the reference beam.

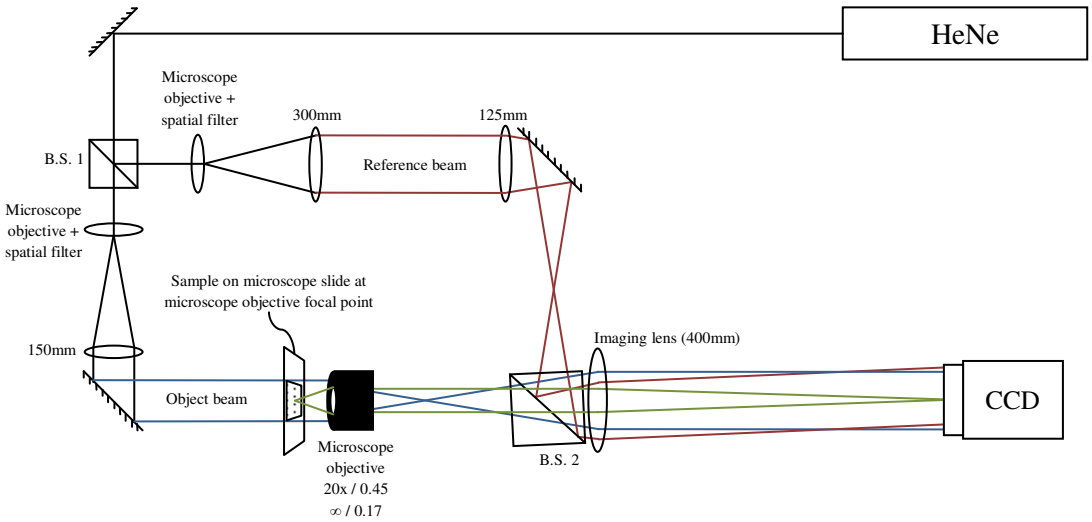

Figure 2.2.1 *Our slightly off-axis microscopic interferometry setup. The sample is placed at the left focal point of the microscope objective and is brought to a focus on the CCD (green). The left focal point of the imaging lens coincides with the right focal point of the microscope objective so that the collimated light from the object beam (red) that enters the microscope objective is re-collimated before falling on the CCD. The reference beam (blue) is also brought to a focus so that the imaging lens collimates it before it falls on the CCD. Drawing not to scale.*

To analyze the effectiveness of this setup, we prepared a solution of silica beads suspended in nanopure water. Then, we added a drop of this solution onto a microscopic slide and placed that in the object beam. Figure 2.2.2 shows an isolated silica sphere we captured with the expected interference pattern.

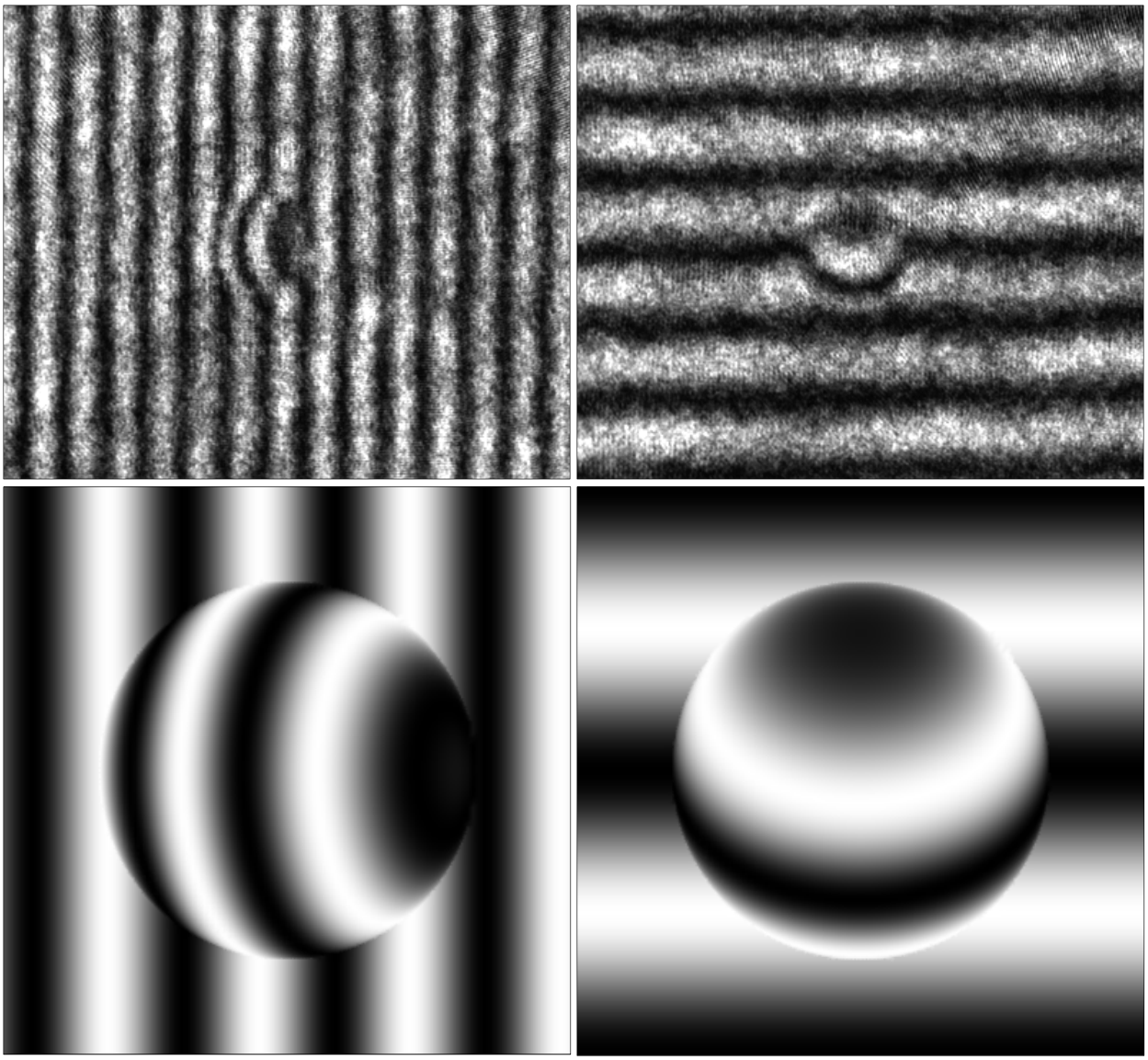

Figure 2.2.2 *Real and simulated images of a single isolated silica sphere suspended in water. The top row shows actual captures and the bottom row shows simulated images. The left images show deflected vertical fringes while the right images show deflected horizontal fringes.*

The fringes are deflected along the sphere as in the simulated image in figure 1.3.2. As before, we may calculate the optical thickness of the sphere and from that the diameter of the sphere using the known refractive index of silica glass and by counting the number of fringes the interference pattern is shifted by.

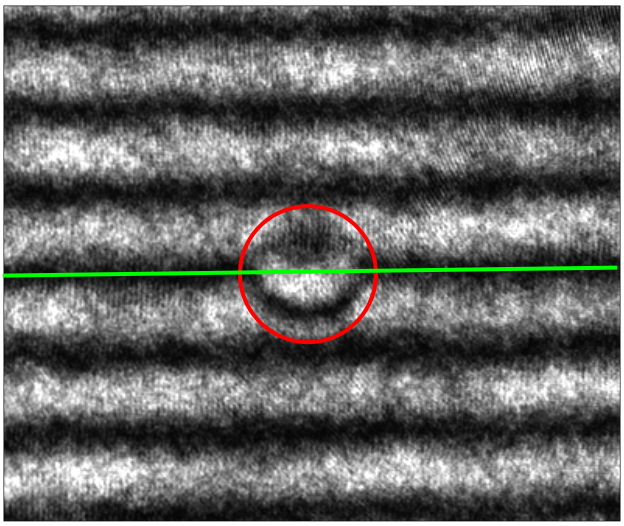

Figure 2.2.3 *5 micron silica sphere with overlaid lines to indicate the introduced phase shift*

From the image, we measured an approximate phase shift of 1.5π radians or 0.75 cycles. The wavelength of our HeNe was 633nm. The refractive index of water at 633nm is 1.33. The refractive index of the silica spheres according to Bangs Laboratories Product Data Sheet 702 for Uniform Silica Microspheres is between 1.43 and 1.46. Plugging the extremes of the refractive index into equation 1.4 yields

$$d_{1.43} = \frac{(0.75)(633 \times 10^{-9})}{1.43 - 1.33} = 4.75\mu m$$
$$d_{1.46} = \frac{(0.75)(633 \times 10^{-9})}{1.46 - 1.33} = 3.65\mu m$$

which has an average of

$$d = (4.2 \pm 0.5)\mu m$$

The spheres we used were 4.74µm in diameter, so this result is in good agreement with what we would expect. It is difficult to measure precisely the number of cycles by which the phase was retarded. One method to determine the phase shift more precisely is discussed in section 4.

Without knowing the refractive index of the material, it is still possible to measure the optical thickness of the object and get an idea of the shape of the object. One possible application of this method involves imaging biological cells. Figure 2.2.4 shows the interference pattern formed when introducing a buccal epithelial cell into the object beam. The interference fringes in the center of the cell are deflected more than those on the edges suggesting the cell is optically deeper at the center. Given the known shape of this type of cell, this is not surprising. It is also possible to highlight the cell by adjusting the angle between the object and reference beam so that they are parallel. Figure 2.2.5 shows this effect. The cell may be imaged easily without staining.

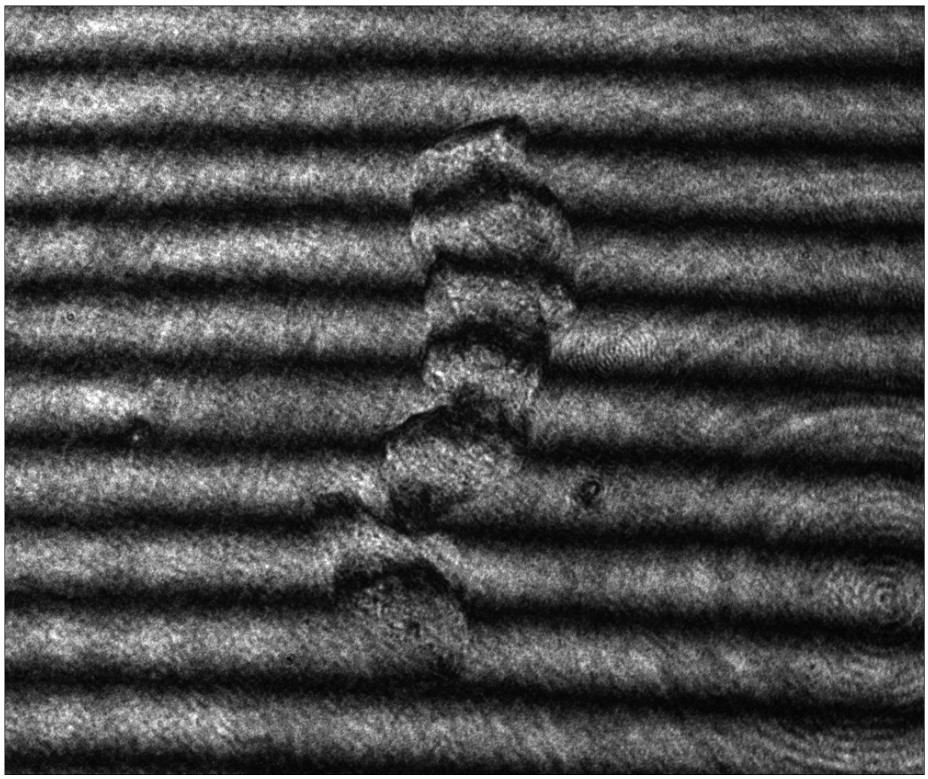

Figure 2.2.4 *Buccal epithelial cell with interference pattern overlay.*

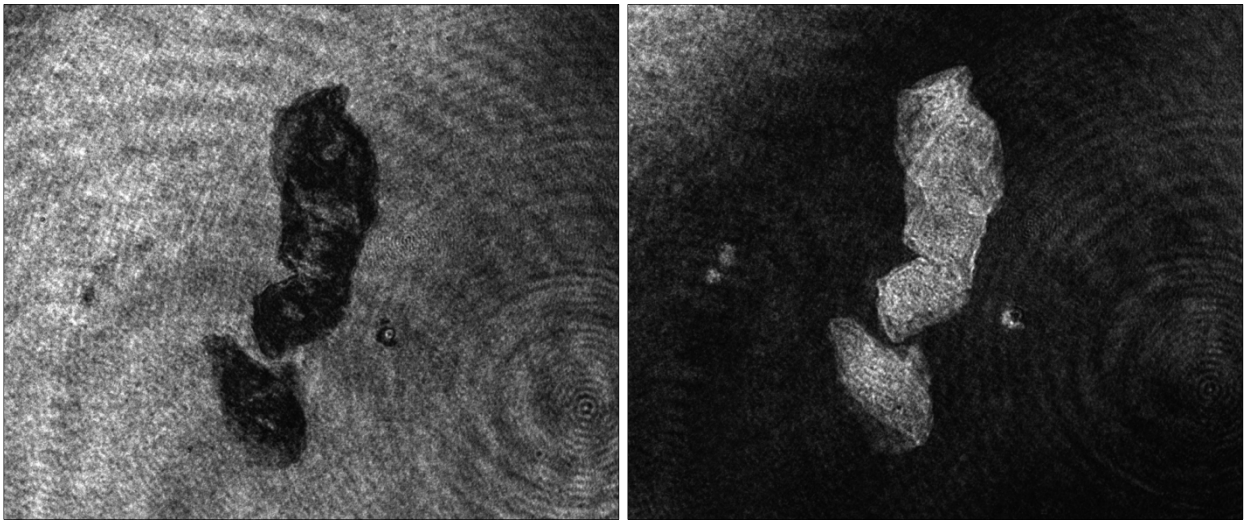

Figure 2.1.5 *Two images of the same buccal epithelial cell from figure 2.2.4 but with very wide fringes. The cell stands out clearly from the background without staining.*

3. Conclusion

We were able to capture a number of well formed holograms using our setup and we were able to reconstruct them using numerical methods based on the Fresnel-Kirchhoff integral and work

done by Schnars and Jüptner. We were also able to resolve multiple focal planes of a 3-D sample using a single hologram.

Using related concepts and techniques, we were able to build an optical interferometry setup and get a rough estimate of the optical thickness of 5µm silica spheres that agreed closely with the manufacturer's specifications. We were also able to image buccal epithelial cells and demonstrate the use of phase shifting techniques to highlight those biological cells against their surroundings.

4. Possible Further Research

4.1. Continuous Phase Shifting using liquid-crystal device

One difficulty we encountered when attempting to measure the optical thickness of the silica spheres involved determining the phase shift introduced by the sample. One possible solution could involve the use of a continuous phase shifting liquid-crystal device. In this setup, a phase shifting liquid crystal device would be placed in the path of the reference beam. Adjusting the phase of the reference beam through one cycle would cause each pixel to go through one cycle of dark-light-dark or light-dark-light. Using several sequential images of the interferogram, each with a further phase shift, one could determine more accurately the phase shift of each pixel. Knowing the phase shift accurately, one could then more precisely determine the optical thickness of the sample at that point and potentially obtain an optical thickness profile for the sample.

Appendix A – proc_hol_schnars.m

```
colormap gray;

% Image Definitions
imgsrc='Images/USAF-hologram.png';
imgw=2448;
imgh=2050;
pxpt=3.45e-6; % Pixel size in meters

% Scan for 1st order
scan_start=0.25850-0.02;
scan_end=0.25850-0.01;
scan_int=0.01;

% Full Frame
%frame_xrange=1:imgw;
%frame_yrange=1:imgh;

% 1st Order medium
frame_xrange=672:930;
frame_yrange=913:1110;

lambda=0.633e-6;
ii=sqrt(-1);

% Load the image
im=imread(imgsrc);
imagesc(im)
im=double(im);

for z=scan_start:scan_int:scan_end;
    % Figure the transfer function from Schnars 2002
    del_x=pxpt; del_y=pxpt;
    H=zeros(imgh,imgw);
    for i=1:imgh;
        for j=1:imgw;
            r2=((i-(imgh/2))*del_x)^2+((j-(imgw/2))*del_y)^2;
            H(i,j)=exp((-ii*pi/(z*lambda))*r2);
        end
    end

    gam=fft2(im.*H);
    gam=ifftshift(gam);
    gg=gam.*conj(gam);
    %imagesc(log(1+gg(frame_yrange,frame_xrange)));
    imagesc(sqrt(1+gg(frame_yrange,frame_xrange)));
    %imagesc(gg(frame_yrange,frame_xrange));

    text(10,10,strcat('\color{white}z=',sprintf('%3.0f%',z*1000),'mm'));

    drawnow;
end
```

Appendix B – Mathematica unobstructed interference pattern code

```
DensityPlot[Cos[x], {x, -15 π, 15 π}, {y, -15 π, 15 π},
 PlotPoints → 50,
 ColorFunction → GrayLevel,
 Frame → None
]
```

Appendix C – Mathematica transparent spherical sample interference pattern code

```
r = 10 π;
p[x_, y_] = If[x^2 + y^2 < r^2, 3 π / r √(r^2 - x^2 - y^2), 0];
Show[
 DensityPlot[Cos[x - p[x, y]], {x, -15 π, 15 π}, {y, -15 π, 15 π},
  PlotPoints → 100,
  ColorFunction → GrayLevel,
  Frame → None
 ],
 Graphics[{
   Thick, Red, Line[{{0, 15 π}, {0, -15 π}}],
   Green, Line[{{-15 π, 0}, {15 π, 0}}]
  }]
]
```

- **Capture Device**

Basler piA2400-17gm http://www.graftek.com/pdf/Brochures/basler/pilot_1.pdf	
Sensor Size (H x V pixels)	2448 x 2050
Pixel Size (µm)	3.45 x 3.45
Max. Frame Rate (at full resolution)	17 fps
Data Output Type (Interface)	Gigabit Ethernet (GigE Vision compliant)

- **Capture Software**
  - National Instruments Measurement & Automation Explorer
- **Central Processing Unit**
  - Intel® Pentium® 4 CPU 3.80GHz (2 CPUs)

References

[1] Ulf Schnars and Werner P O Jüptner "Digital recording and numerical reconstruction of holograms," *Meas. Sci. Technol*, Vol. 13, Issue 9 (2002)

[2] N. Shaked, Y. Zhu, M. Rinehart, and A. Wax, "Two-step-only phase-shifting interferometry with optimized detector bandwidth for microscopy of live cells," *Optics Express*, Vol. 17, Issue 18, pp. **15585-15591** (2009)